



Published in final edited form as:

Nat Neurosci. 2009 November ; 12(11): 1398–1406. doi:10.1038/nn.2410.

The oligodendrocyte-specific G-protein coupled receptor GPR17 is a cell-intrinsic timer of myelination

Ying Chen¹, Heng Wu¹, Shuzong Wang¹, Hisami Koito², Jianrong Li², Feng Ye¹, Jenny Hoang¹, Sabine S. Escobar³, Alex Gow⁴, Heather A. Arnett³, Bruce D. Trapp⁵, Nitin J. Karandikar⁶, Jenny Hsieh⁷, and Q. Richard Lu^{1,6,7,#}

¹Department of Developmental Biology and Kent Waldrep Foundation Center for Basic Neuroscience Research on Nerve Growth and Regeneration, University of Texas Southwestern Medical Center, Dallas, TX 75390, USA.

²Department of Veterinary Integrative Biosciences, Texas A&M University College Station, Texas 77843, USA.

³Department of Inflammation, Amgen, Seattle, WA 98119, USA

⁴Center for Molecular Medicine and Genetics, Wayne State University, Detroit, Michigan 48201, USA.

⁵Department of Neurosciences, Lerner Research Institute, Cleveland Clinic, Cleveland, OH 44195, USA

⁶Department of Pathology, University of Texas Southwestern Medical Center, Dallas, TX 75390, USA.

⁷Department of Molecular Biology, University of Texas Southwestern Medical Center, Dallas, TX 75390, USA.

Abstract

The bHLH transcription factor Olig1 promotes oligodendrocyte maturation and is required for myelin repair. In this report, we characterize an Olig1-regulated G-protein coupled receptor GPR17 whose function is to oppose the action of Olig1. *GPR17* is restricted to oligodendrocyte lineage cells but downregulated during the peak period of myelination and in adulthood.

Transgenic mice with sustained *GPR17* expression in oligodendrocytes exhibit stereotypic features of myelinating disorders in the CNS. *GPR17* overexpression inhibits oligodendrocyte differentiation and maturation both *in vivo* and *in vitro*. Conversely, *GPR17* knockout mice display early onset of oligodendrocyte myelination. The opposing action of *GPR17* on

Users may view, print, copy, download and text and data-mine the content in such documents, for the purposes of academic research, subject always to the full Conditions of use: http://www.nature.com/authors/editorial_policies/license.html#terms

#Corresponding author, qrichard.lu@utsouthwestern.edu Tel: 214-648-7410; Fax: 214-648-1960.

Author contributions:

Q.R.L. designed the study, analyzed the data and coordinated the project. Y.C. performed the analysis of transgenic and knockout mice, and immunohistological and biochemical assays. H.W. generated *GPR17* knockout mice. S.W. performed initial gene analysis and assisted the generation of *GPR17* transgenic mice. H.K. and J.L. performed OPC transfection and analysis. F.Y. and J.H. performed *in situ* hybridization and ChIP assay. S.S.E. and H.A.A. analyzed MS samples. A.G. performed cell death assay. B.D.T. analyzed MS samples and contributed conceptually to the project. N.J.K. provided EAE mice. J.H. provided HCN cells and performed biochemical assays. Q.R.L. and Y.C. wrote the manuscript.

oligodendrocyte maturation reflects, at least partially, upregulation and nuclear translocation of the potent oligodendrocyte differentiation inhibitors ID2/4. Collectively, these findings suggest that GPR17 orchestrates the transition between immature and myelinating oligodendrocytes via an ID protein-mediated negative regulation, and may serve as a potential therapeutic target for CNS myelin repair.

Keywords

oligodendrocyte differentiation and myelination; G-protein coupled receptor; *Olig1*; demyelinating diseases; ID proteins; multiple sclerosis

Introduction

Myelination by oligodendrocytes is essential for the normal function of the vertebrate central nervous system (CNS). Demyelination or dysmyelination disrupts saltatory nerve conduction, leading to axonal degeneration and neurological disabilities associated with acquired and inherited disorders such as multiple sclerosis (MS) and leukodystrophies 1, 2. At present, molecular mechanisms underpinning oligodendrocyte myelination and remyelination after injury are poorly understood. In rodents, oligodendrocyte precursor cells (OPCs) initially form during embryonic stages, but they do not generate myelin-producing oligodendrocytes until perinatal stages 3. This likely reflects a highly coordinated process of myelination, in which positive and negative factors modulate the timing of oligodendrocyte maturation with final myelination of axons being actively opposed until all neuronal components of the developing CNS are in place.

Extracellular signals and intracellular timers including oligodendrocyte differentiation inhibitors (e.g. ID2 and ID4) 4, 5 and cell cycle inhibitors (p21, p27 and p57) 6–8 are shown to regulate oligodendrocyte maturation. Several receptor-mediated signaling pathways have been found critical for oligodendrocyte differentiation/myelination, including signaling mediated by Notch, BMP, neuregulin/ErbB2 and Lingo-1 9–14. However, signaling mechanisms that mediate the operation of intracellular inhibitors or timers for the transition from immature to mature myelinating oligodendrocytes remain elusive. The observation that OPCs are present within demyelinating MS lesions but fail to differentiate into mature oligodendrocytes 15, 16, suggests that the remyelination process is blocked at a premyelinating stage in demyelinating lesions. Thus, identification of critical regulators that inhibit myelination/remyelination could facilitate the development of therapeutic targets for myelin repair in CNS demyelinating diseases.

The basic helix-loop-helix (bHLH) transcription factors *Olig1/2* play an important role in oligodendrocyte myelination and remyelination 17–21. While *Olig2* directs multipotent neural stem/progenitors to become lineage-restricted OPCs, *Olig1* promotes maturation of oligodendrocytes in the developing CNS and is required for repair of demyelinated lesions in a murine model of multiple sclerosis 18, 19, 22. Through transcriptome profile analysis of *Olig1* null CNS 19, we identified an oligodendrocyte lineage specific G-protein coupled receptor, GPR17. By analyzing *GPR17* overexpressing transgenic and knockout mice, we demonstrate that *GPR17* negatively regulates oligodendrocyte differentiation and

myelination *in vitro* and *in vivo*. Hence, our studies suggest that *GPR17* functions as a potent negative regulator for oligodendrocyte myelination, at least in part, via inducing nuclear localization of differentiation inhibitors ID2/4 and opposing *Olig1* function.

Results

Identification of oligodendrocyte lineage-specific *GPR17*

To identify the factors that may regulate oligodendrocyte myelination, we screened for genes downregulated in the optic nerves of myelination-deficient *Olig1* null mice using differential display 23 and microarray analysis (Supplementary Table 1). Among genes downregulated or absent in *Olig1* mutants, *GPR17* expression was reduced approximately 232 folds from gene chip microarray analysis. Northern blot analysis (Fig. 1a) indicated that *GPR17* is essentially absent from *Olig1* null brains. Multiple Tissue Northern blot analysis showed that *GPR17* is restricted to the rodent CNS (Fig. 1b). Mouse *GPR17* encoding a 339 amino acid residue protein with typical rhodopsin P2Y type-seven transmembrane motifs 24 is highly conserved among vertebrate species (Supplementary Fig. 1).

In the spinal cord, expression of *GPR17* was initially detected in the ventral ventricular zone at e15.5 (Fig. 1c), which coincided with the appearance of a myelin gene *Plp1/DM20* (Fig. 1d). At the late embryonic stage e18.5, *GPR17* expression appeared throughout the gray and lateral white matter (Fig. 1e). In contrast, *GPR17* was not observed in peripheral Schwann cells in the dorsal root ganglion (Fig. 1d vs. c, arrowheads).

At P14, *GPR17*⁺ cells were enriched in CNS white matter tracts (Fig. 1f–k). They were also detected in gray matter regions (Fig. 1i–j, arrowheads). To define the identity of *GPR17*⁺ cells, we performed double *in situ* hybridization of *GPR17* with markers for oligodendrocytes or their precursors. Approximately 79% *GPR17*⁺ cells expressed *Plp1* in the corpus callosum and cortex at P14 (Fig. 1g; Supplementary Fig. 2), while a subset of them (approximately 21%) expressed an OPC marker *Pdgfra* (Fig. 1h, Supplementary Fig. 2). Thus, these data suggest that *GPR17* is primarily, if not only, expressed in cells of the oligodendrocyte lineage. Consistent with its oligodendrocyte-specific expression, *GPR17* was essentially undetectable in CNS regions of *Olig1* mutants (Fig. 1 l–n).

GPR17 is downregulated in mature oligodendrocytes

In the developing spinal cord, *GPR17*⁺ cells appeared to increase from P0 to P7 (Fig. 2a,b), similar to that of *Olig2*⁺ cells (Fig. 2). At P14, the number of *GPR17*⁺ cells in the white matter was reduced as compared to that at P7 (Fig. 2). Strikingly, *GPR17*⁺ cells decreased drastically beginning at P21 (Fig. 2d), the peak period of myelinogenesis 25. They were barely detectable in adulthood (Fig. 2e), in contrast to the continuous presence of *Olig2* or *Olig1*-expressing cells (Fig. 2i,j; Supplementary Fig. 3; data not shown). This age-dependent reduction of *GPR17* expression was further confirmed by quantitative real time PCR (qRT-PCR) and Western blot analyses (Fig. 2k,n), suggesting that *GPR17* is downregulated during terminal oligodendrocyte maturation. In contrast, expression of mature oligodendrocyte makers *Mbp* and *CC1* was highest at P21, and persisted to adulthood (Fig. 2l, data not shown).

To determine whether *GPR17* expression can be directly regulated by *Olig1*, adult hippocampus-derived neural stem/progenitors (HCN) were transfected with *Olig1* and the cells were allowed to differentiate into oligodendrocytes in the presence of IGF-1 26. Consistent with the role of Olig1 in promoting oligodendrocyte differentiation, we observed an increase of myelin gene expression in *Olig1*-transfected cells, whereas the level of *GPR17* was significantly reduced (Fig. 2o). Similar results were observed in *Olig2*-transfected cells (Fig.2o). To understand the molecular basis of Olig1-mediated repression of *GPR17*, we then asked whether Olig1 could directly bind to the E-box consensus sequence (CANNTG) in the upstream regulatory region of *GPR17* (Fig. 2p). Chromatin immunoprecipitation (ChIP) was performed using an antibody against Myc-tagged Olig1 in transfected cells. DNA fragments from the immunoprecipitated chromatin of *Olig1*-transfected cells could be amplified with the primers flanking the promoter region containing an E-Box consensus sequence of the bHLH factor-binding motif, but not with the primers for the region lacking the consensus sequence (Fig. 2p). We detected an increase of Olig1 recruitment to the *GPR17* regulatory region containing the potential Olig1 binding site in *Olig1* transfected cells compared to vector transfected cells (Fig. 2q). These observations suggest that Olig1 can physically bind to the promoter of *GPR17* and negatively regulate its expression.

***GPR17* is upregulated in demyelinating lesions in the CNS**

Since a low level of *GPR17* is detected in adult spinal cord, we then examined *GPR17* expression after demyelination injury induced by EAE, a mouse model of MS. EAE was induced in adult C57/BL6 mice by MOG35-55/CFA immunization. Spinal cords of control CFA-immunized mice or EAE mice with varying degrees of disease severity were dissected and processed for H/E analysis (Supplementary Fig. 4a–d). Inflammatory demyelinating lesions in the spinal cord were associated with prominent inflammatory infiltrate, where *Mbp* expression was reduced significantly or absent (Supplementary Fig. 4). In contrast to scattered *GPR17*⁺ cells in controls, the number of *GPR17*⁺ cells markedly increased at the demyelinating lesion penumbra and/or within the lesion (Supplementary Fig. 4). *GPR17* expression was upregulated mainly in *Olig1*⁺ cells and a subset of *Pdgfra*⁺ OPCs in these lesions (Supplementary Fig. 4m,n). Thus, while downregulated in normal adult spinal cord, *GPR17* is re-expressed or upregulated in oligodendroglial cells after EAE-induced demyelinating injury.

qRT-PCR analyses of a cohort of human MS tissues indicate that a significantly higher level of expression of *GPR17* was detected in MS plaques as compared to the white matter from non-neurological donor samples and normal-appearing white matter from MS donors (Supplementary Fig. 4o,p). Thus, *GPR17* upregulation appears to be associated with demyelinating lesions induced by EAE and in MS.

Generation of *GPR17* overexpressing transgenic mice

The fact that *GPR17* expression is downregulated during active myelinogenesis and upregulated in demyelinating lesions raises a possibility that sustained expression of *GPR17* may negatively regulate oligodendrocyte myelination. To test this possibility we generated transgenic mice with *GPR17* expression under the control of an oligodendrocyte-expressing

CNPI promoter. We included a Myc tag to follow *GPR17* transgene-expressing cells (Supplementary Fig. 5a).

qRT-PCR and Western blot analyses revealed that expression of *GPR17* transcript and protein in the brain of transgenic mice at P12 is approximately six and three fold higher than that of control littermates, respectively (Supplementary Fig. 5b,c). Myc tagged-GPR17 immunostaining was mainly detected in CC1+ differentiated oligodendrocytes, but not in PDGFR α + OPCs in this transgenic line (Supplementary Fig. 5d–h). Multiple parallel processes along axons were visualized in Myc-GPR17+ oligodendrocytes (Supplementary Fig. 5i). In contrast, there was no overlap between Myc-GPR17 and the astrocyte marker GFAP or the pan-neuronal marker NeuN (Supplementary Fig. 5j,k). Thus, these data indicate that the *GPR17* transgene is predominantly expressed in oligodendrocytes after the precursor stage.

Sustained expression of *GPR17* inhibits CNS myelination

Starting at postnatal week two, *GPR17* transgenic animals began to exhibit generalized tremors, hindlimb paralysis and seizures (data not shown), reminiscent of those described for dysmyelinating mouse mutants 27. The severity of tremors increases during the postnatal week three and the majority of transgenic mice died around this period (Fig. 3a). In *GPR17* transgenic animals, we observed a significant reduction of *Mbp* and *Plp1* expression in the cerebral white matter region at P14 (Fig. 3b,d). At P20, the reduction was much more severe (Fig. 3c,e), suggesting that myelin gene expression decreases progressively with age. The marked reduction of myelin gene expression was confirmed by immunostaining for MBP (Fig. 3g) and Western blot analysis (Fig. 3h). O4 immunostaining, which detects both pre- and differentiated oligodendrocytes, showed decreased immunoreactivity in the corpus callosum of transgenic mice due to the reduction of mature oligodendrocytes (Fig. 3i). This observation suggests that *GPR17* overexpressing cells at the O4+ stage do not differentiate further and/or undergo cell death.

By qRT-PCR analysis for expression of various myelin genes in the transgenic cortices, we observed a significant decrease of myelin gene expression at P20 but not at an early developmental stage P7 (Figure 3j,k). Similar results were also obtained by quantifying *Plp1*+ oligodendrocytes in the CNS (Supplementary Fig. 6). In addition, we did not observe any detectable neuronal cell death and axonal loss in transgenic mice at P7 (data not shown).

Despite the deficiency in oligodendrocyte myelination, OPCs formed in the transgenic brain were comparable to the control (Fig. 3l, m). Furthermore, using BrdU incorporation and Ki67 to detect proliferating OPCs, we did not detect significant alteration of OPC proliferation rates in the brain at different developmental stages (Fig. 3n; data not shown). These observations suggest that despite initial formation of OPCs at early postnatal stage, oligodendrocyte myelination is likely arrested at or after a pre-myelinating stage in *GPR17*-overexpressing animals.

In contrast to markedly reduced myelin gene expression, expression of an astrocytic marker GFAP was upregulated in the CNS of transgenic mice (Fig. 3f,h). However, the number of astrocytes marked by glutamine synthetase28 was similar to control (data not shown),

indicating an astroglial response to hypomyelination. Consistent with this notion, we observed substantial Iba1+ activated microglia/macrophages with a hyper-ramified morphology in the transgenic brain (Supplementary Fig. 7).

Myelination defects were also evident in the spinal cord of transgenic mice (Supplementary Fig.8). In contrast to the widespread CNS myelination deficiency, myelinogenesis appeared normal in the peripheral nervous system such as in the sciatic nerve (data not shown), suggesting that myelination defects caused by *GPR17*-overexpression are specific to the CNS.

Myelinogenesis deficiency in *GPR17*-overexpressing mice

In *GPR17* transgenic mice at P19, optic nerves were translucent compared to WT littermates (Fig. 4a), indicating a lack of myelin sheaths. The number of myelinated axons was much reduced in CNS regions (Fig. 4b). Ultrastructural analysis revealed that myelinogenesis is essentially absent in the optic nerve, corpus callosum and spinal cord (Fig. 4c). The reduction of myelin thickness or absence of myelin was observed for all axons independent of their caliber size. These results suggest that myelination is generally defective in the CNS with *GPR17* overexpression in CNP+ oligodendrocytes.

Although a few myelinated axons were observed in the optic nerve of transgenic mice at P14 (Fig. 4d), they were hardly detectable at P21 (Fig. 4d). This is correlated with a reduction in the number of mature oligodendrocytes and myelin gene expression at later developmental stages (Fig. 4f,g), suggesting a loss of mature myelinating oligodendrocytes after prolonged *GPR17* overexpression.

Comparing with morphologically normal oligodendrocytes surrounded by myelinated axons (arrows) in the optic nerve from WT mice (Fig. 4e), many oligodendrocytes in *GPR17* transgenic mice contained condensed chromatin mass and shrunken cytoplasm (Fig.4e, arrow), a characteristic feature of cells undergoing apoptosis. In contrast, we did not detect oligodendrocyte death in age-matching wildtype mice. Thus, these observations suggest that sustained *GPR17* overexpression in CNP+ oligodendrocytes leads these cells to differentiation arrest and/or apoptotic cell death. Despite the deficits in mature oligodendrocytes, we did not observe significant neuronal cell death (data not shown) and axonal loss as detected by neurofilament immunostaining (Fig. 4h).

GPR17 overexpression inhibits oligodendrocyte maturation

To determine the effects of *GPR17* expression on oligodendrocyte differentiation *in vitro*, we transfected *GPR17*-expressing and control vectors carrying a nuclear localized GFP 30 in HCN progenitors 26. At 3 days post-transfection, control transfected cells differentiated into mature oligodendrocytes exhibiting elaborated complex processes and expression of mature oligodendrocyte markers RIP, MBP and MOG (Fig. 5a). In contrast, *GPR17*-overexpressing cells presented as a simple bi- or tri-polar morphology lack of expression of mature oligodendrocyte markers (Fig. 5b), suggesting that they were arrested at the precursor stage.

In light of negative effects of *GPR17* on oligodendrocyte differentiation, we then examined whether *GPR17* overexpression could alter expression of potential oligodendrocyte differentiation inhibitors such as *ID2*, *ID4*, *Hes5* and *Tcf4/Tcf712* 4, 5, 14, 31. By qRT-PCR assay, we detected a significant increase of *ID2* but not *ID4*, *Tcf4* and *Hes5* (Fig. 5c). Strikingly, in contrast to cytoplasmic expression of *ID2* in control-transfected cells (Fig. 5d), *ID2* appeared to translocate into the nucleus in the majority of *GPR17*-transfected cells (Fig. 5e; Supplementary Fig. 9g). By fractionating nuclear and cytoplasmic components of *GPR17*-transfected cells, we observed predominantly nuclear accumulation of *ID2* with a concomitant decrease in the cytoplasm (Fig. 5f). As controls, *GPR17* overexpression had no effects on subcellular distribution of a nuclear-localized cAMP response element-binding protein (CREB) and a cytoplasmic-localized protein GAPDH (Fig. 5f). Similarly, *GPR17* overexpression in HCN cells leads to nuclear translocation of *ID4* (Supplementary Fig. 9). Thus, *GPR17* overexpression results in not only an increase of *ID2*, but also nuclear translocation of *ID2/4*, which have been shown to inhibit OPC maturation^{4, 5}.

We further examined the effect of *GPR17* overexpression in primary OPCs isolated from rat neonate cortices. The formation of complex MBP⁺ cells among GFP⁺ cells is significantly reduced from ~43% in the control to ~22% in *GPR17*-transfected OPCs (>1000 cell counts, $p < 0.01$). *GPR17*-transfected cells appeared to have less or thin processes (Fig. 5h), suggesting that *GPR17* overexpression inhibits OPC maturation *in vitro*.

To define the differentiation potential of *GPR17*-overexpressing cells, we prepared oligodendroglial enriched cultures from embryonic cortices. Although O4⁺ pre-oligodendrocytes were detected in the culture from transgenic embryos, they failed to fully differentiate into complex MBP⁺ oligodendrocytes, in contrast to the formation of mature MBP⁺ oligodendrocytes in WT culture (Fig. 5i). *ID2* expression was observed in the cytoplasm of mature oligodendrocytes in WT culture, while it was detected in the nucleus of immature oligodendrocytes cultured from *GPR17* transgenic animals (Fig. 5j).

Consistent with the *in vitro* results, we detected an upregulated expression level of *ID2* in the corpus callosum of transgenic mice (Supplementary Fig. 10). To determine whether *ID2* can be associated with Olig1 and therefore block Olig1 function in *GPR17* overexpressing cells, we performed co-immunoprecipitation (Co-IP) assays with *ID2* and Olig1 using oligodendroglial cells-enriched culture from WT, *GPR17*-overexpressing transgenic mice and *GPR17* null mutants. We observed that less Olig1 was pulled down by *ID2* from Co-IP of *GPR17* null cells when compared to WT, while in *GPR17*-overexpressing cells, significantly higher amount of Olig1 was associated with *ID2* (Fig. 5k). A similar result was also obtained in an *ID4*/Olig1 Co-IP pull-down assay (Fig. 5k). These observations suggest that *GPR17* induces nuclear localization of differentiation inhibitors such as *ID2/4*, which then inhibit oligodendrocyte maturation by sequestering Olig1 through direct interactions.

***GPR17* null mice exhibit early onset of CNS myelination**

To study the effects of the loss-of-function of *GPR17*, we generated *GPR17* null mice by homologous recombination in embryonic stem cells. Our targeting strategy deleted the entire *GPR17* coding region (Fig. 6a). The targeted allele was confirmed by Southern blotting and PCR analyses (Fig. 6b,c). Histone 2b fused GFP (h2b-GFP) was knocked into the *GPR17*

locus to trace individual endogenous GPR17 expressing cells (Fig. 6a). Double immunostaining of GFP with a battery of markers for oligodendrocyte lineage cells, astrocytes and neurons demonstrated that *GPR17* is restricted to the oligodendrocyte lineage (Supplementary Fig. 11 – Supplementary 14), consistent with observations with mRNA in situ hybridization. Similarly, *in vitro* studies with oligodendroglial cultures isolated from *GPR17*^{+/-} embryonic cortices indicated that GPR17 was detected in PDGFR α ⁺ OPCs and MBP⁺ mature oligodendrocytes (Supplementary Fig. 15).

Consistent with a role for GPR17 in inhibiting maturation of oligodendrocytes, early and robust MBP expression was already detectable in the spinal cord of *GPR17* null embryos at e17.5 (Fig. 6e). In contrast, MBP expression was barely detectable in the spinal cord of control embryos at this stage (Fig. 6d), despite a comparable formation of PDGFR α ⁺ OPCs and their proliferation rate between control and null mice (Fig. 6f,g; Supplementary Fig. 16).

Since the initiation of axonal myelination typically occurs at neonatal stages, we then examined myelin formation at P3 by electron microscopy in the spinal cord, where myelination is relatively homogeneous and well characterized. *GPR17*^{-/-} mice exhibited a significant increase in the number of myelinated axons compared to their WT littermates in the corresponding lateral white matter region (Fig. 6h–j), suggesting an early onset of CNS myelination in the absence of *GPR17*.

Adult *GPR17* null mice did not appear to exhibit a significant increase of myelinated axon fibers in the CNS. The myelin g-ratio and the number of oligodendrocytes were comparable between WT and *GPR17* null mice (data not shown). This may likely reflect that there are other regulators for the induction of myelination that can compensate for the loss of *GPR17* in adult mice.

To determine the differentiation capacity of *GPR17*^{-/-} progenitor cells *in vitro*, we cultured oligodendroglial progenitors from WT, *GPR17*^{+/-} and ^{-/-} embryos^{32, 33}. *GPR17*^{-/-} progenitors differentiated into MBP⁺ or RIP⁺ mature oligodendrocytes earlier than control cells (Fig. 6k–n; Supplementary Fig. 17). Despite the initial delay, WT and heterozygous precursors increasingly differentiated into oligodendrocytes over time and eventually reached the same level as *GPR17* null precursors (Fig. 6k–n). Thus, *in vitro* and *in vivo* observations suggest that the loss of GPR17 function accelerates oligodendrocyte precursor differentiation and myelination.

Discussion

GPR17 as a negative regulator of CNS myelination

A precise balance between activators and inhibitors is crucial for controlling the timing of myelination in the CNS under normal and pathological conditions^{34, 35}. A common feature of demyelinated lesions is the differentiation block of oligodendrocyte precursors at a pre-myelinating stage^{36, 37}. Identification and characterization of inhibitory signaling molecules may provide potential therapeutic targets for enhancing remyelination. In this study, we identified a G-protein coupled receptor GPR17 that functions as a negative regulator for CNS myelinogenesis.

GPR17 is restricted to oligodendrocyte lineage cells in the CNS in a developmentally regulated manner. Like other inhibitory factors³⁸, as development progresses, *GPR17* expression is downregulated and oligodendrocyte myelination begins. *In vitro*, *GPR17* overexpression not only blocks differentiation of neural progenitor cells into oligodendrocytes but also inhibits terminal differentiation of primary OPCs. In transgenic mice, sustained *GPR17* overexpression in CNP⁺ oligodendrocytes results in myelination arrest and oligodendrocyte loss. Conversely, *GPR17* deletion accelerates OPC maturation *in vitro* and leads to an early-onset of myelination in the developing CNS. Taken together these data suggest that GPR17 acts to negatively regulate oligodendrocyte differentiation and myelination.

GPR17 was identified as one of the genes downregulated in *Olig1* mutant mice. This is likely due to the reduction of differentiated oligodendrocytes in *Olig1* mutants, resulting in a decrease of many genes expressed in oligodendrocytes (Supplementary Table 1). Nonetheless, overexpression of *Olig1* represses *GPR17* expression by directly binding to its regulatory region, indicating that *Olig1* negatively regulates *GPR17* expression. Of note, the oligodendrocyte-restricted GPR17 expression described here and elsewhere³⁹ is at odds with earlier reports showing that the majority of GPR17⁺ cells are neurons^{40, 41}. This discrepancy may reflect the specificity of GPR17 antibodies used in the earlier studies for immunohistochemistry⁴¹. In the present study, analyses of mRNA and a nuclear-localized GFP reporter for endogenous GPR17 expression clearly demonstrated that GPR17 is expressed predominantly, if not only, in oligodendrocyte lineage cells in the CNS.

A negative regulatory loop modulates CNS myelination

Several potent regulators of the timing of oligodendrocyte differentiation have been identified including the HLH factors ID2, ID4 and Hes5^{4, 5, 14, 31} as well as cell cycle inhibitors^{7, 42–44}. At present, the extracellular signals that control the operation of intracellular inhibitors or timers for oligodendrocyte maturation are not fully understood. We observed that *Olig1* promotes myelin gene expression while repressing *GPR17* expression. Overexpression of *GPR17* inhibits oligodendrocyte differentiation and leads to nuclear localization of ID2/4, the powerful inhibitors of oligodendrocyte maturation^{4, 5}. ID2/4 were shown to physically interact with and sequester the bHLH factors *Olig1* and *Olig2* to block oligodendrocyte differentiation¹⁴. The fact that GPR17 overexpression increases nuclear translocation of ID2/4 and their association with *Olig1* suggests that GPR17 signaling opposes the action of *Olig1* and possibly its paralog *Olig2*, for oligodendrocyte differentiation through an ID protein-mediated negative regulatory loop (Supplemental Fig. 18). The phenotype of *GPR17* overexpression in transgenic mice is reminiscent of that in *Olig1* null mice with severe myelination deficits¹⁹. On the other hand, *GPR17* null mice exhibit accelerated oligodendrocyte differentiation and early onset of myelination. Thus, these gain- and loss-of-function studies suggest that GPR17 is an integral signaling component that controls the timing of oligodendrocyte differentiation and orchestrates the transition between immature and mature myelinating oligodendrocytes via, at least in part, ID2/4-mediated negative regulation.

Implications in CNS demyelinating diseases

GPR17 transgenic mice with persistent *GPR17* overexpression in oligodendrocytes exhibit the stereotypic pathology of myelination disorders with the failure of myelin sheath formation and reactive gliosis. We noted that *GPR17* is re-expressed or up-regulated in demyelinating lesions in EAE and human MS plaques (Supplementary Fig. 4). At present, it is not clear whether upregulation of *GPR17* in demyelinating lesions is correlated with remyelination arrest in MS lesions. It will be of interest to determine if the activation of *GPR17* signaling could inhibit remyelination by oligodendrocytes in the lesions. Conversely, *GPR17* antagonists may promote remyelination.

At present, the physiological ligands for *GPR17* are not fully elucidated. A recent *in vitro* study suggests that *GPR17* responds to two classes of ligands, uracil nucleotides and the inflammatory lipid mediators, cysteinyl-leukotrienes⁴¹. It remains of interest to identify and characterize the signals, such as molecules derived from axons or inflammatory mediators, which may activate *GPR17* signaling to block oligodendrocyte maturation. Intriguingly, knockdown of *GPR17* by antisense technology or antagonists decelerated lesion progression in a rat brain focal ischemia model, suggesting a pathological role for *GPR17* during recovery after stroke⁴¹. Compared to intracellular transcriptional regulators, cell-type specific G-protein coupled receptor mediated signaling pathways are highly amenable to pharmaceutical modulation. Our present study suggests that targeted inhibition of *GPR17* receptor signaling together with other treatments might augment remyelination by immature oligodendrocytes following a variety of pathological insults.

Methods

Tissue collection and RNA in situ hybridization

Brains, spinal cords and optic nerves at various stages were harvested, fixed in 4% paraformaldehyde at 4°C overnight, infused with 25% sucrose in PBS overnight, embedded in OCT and cryosectioned at 16 µm. Digoxigenin-and/ or fluorescein-labeled riboprobes were used to perform RNA *in situ* hybridization, as described previously²¹. For double *in situ*, the second probe was developed with Tyramide amplification system (PerkinElmer, Inc.). The probes used were: murine *GPR17*, *Pdgfra*, *Plp1/Dm-20* and *Mbp*. Detailed protocols are available upon request.

Northern blot and quantitative real time polymerase chain reaction (qRT-PCR)

Northern blotting was performed as previously described⁴⁵. qRT-PCR was performed using the ABI Prism 7700 Sequence Detector System (Perkin-Elmer Applied Biosystems) as previously described with *Gapdh* (glyceraldehyde-3-phosphatase dehydrogenase, TaqMan kit, Applied Biosystems) as an internal control¹⁹. Primer sequences used for expression analyses are Rat *Id2* forward 5'- atggaatcctgcagcagctcatc, reverse 5'- acgtttggttctgtccaggtctct; Rat *Id4* forward 5'- actgtgctgcagtcgatatgaa, reverse 5'- tgcaggatctccatttctgctgact; Rat *Mag*: forward 5'- acagcgtcctggacatcatcaaca -3', reverse 5'- atgcagctgacctctacttccgtt -3'; Rat *Cgt*: forward 5'- agataaagatggcgccgttact -3', reverse 5'- tatttgagtgctcctgccggta -3'; Rat *Mbp* forward 5'- ttgactccatcggcgcttcttta -3', reverse 5'- gctgtgccacatgtacaaggactca -3'; Rat *Cnp* forward 5'- tggagaaggacttctgccacttt -3', reverse 5'-

tggaggagctgggaatcacaagct -3'; Rat *Plp* forward 5'- tcttggcgactacaagaccacca -3', reverse 5'- gttccagaggccaacatcaagctcat -3'; Mouse *Mbp*: forward 5'- tcacagaagagacctcaca-3', reverse 5'- gccgtagtgggtagttcttg -3'; Mouse *Gpr17*: forward 5'- acacagttgtctgctgcaa -3', reverse 5'- tgaccgtggtgatgaatggg -3' ; Mouse *Plp*: forward 5'- tgctcgctgtacctgtgtacatt-3', reverse 5'- tacattctggcatcagcgcagaga-3'; Mouse *Cnp*: forward 5'- tccacagtgcaagacgctattca -3', reverse 5'- tgtaagcatcagcggacaccatct -3'; Mouse *Cgt* : forward 5'- tgggtaagtggctcaggaacat -3', reverse 5'-tcctgccagtttggcaatgct -3'; Mouse *Mag*: forward 5'- tggtgtggctgagaaccagtat -3', reverse 5'-tgcacagtgactccagaaggat -3'.

Generation of GPR17 transgenic mice

An MBP enhancer in a pMG2 vector 46 was replaced with a 4.0-kb *CNPI* promoter, which has previously been shown to direct transgene expression specifically in oligodendrocytes in the CNS 47. The *GPR17* coding region with an N-terminal Myc-tag was inserted after the *CNPI* promoter. The NotI fragment carrying the transgene was purified by elutip-D columns and injected into fertilized mouse eggs to produce transgenic founders. All viable founder mice appeared to be mosaic and fertile, however, their progeny developed severely myelination deficits. Tissues of progeny were collected at different stages and processed for various assays such as immunocytochemistry, Western blot and electron microscopic analysis. Progeny from three founder mice carrying *GPR17* transgene gave rise to the same dysmyelinating phenotype. The data presented are derived from the progeny of a single transgenic line.

Generation and genotyping of GPR17 knockout mice

To construct the *GPR17* targeting vector, a 10.1 kb *Sna*B1 genomic fragment was cloned into pKO-915 (Stratagene) vector carrying the DTA gene. In a homologous recombination event, an h2bGFP/neo (neomycin-resistance gene) cassette replaced entire *GPR17* coding exon. H2bGFP protein expression is in-frame fused to the *GPR17* coding region immediately after the translation start site and is under the control of endogenous *GPR17* promoter. This construct was used to target the *GPR17* locus in SM-1 (129/Sv) embryonic stem cells. Correctly targeted cells were confirmed by Southern blotting and were injected into blastocysts to generate chimeric mice. Chimeras were crossed to C57Bl/6 mice to generate germ-line transmitted heterozygous mice. *GPR17* null mice appear normal and were fertile without obvious motor or behavior abnormalities. Genotypes were determined by PCR of tail DNA (*Gpr17*-wt: forward 5'- ctgcttctaccttctggaactcatc-3', reverse 5'- aggtgagcatagagaggtcttcga -3'; *Gpr17*-ko: forward 5'- cttgtgcaacttgctctgcagca-3', reverse 5'- caccagtggaagtcactgagtgtct -3') and yielded 310-bp wild-type and 380-bp mutant allele products, respectively.

Neural stem/progenitor cell culture and oligodendroglial culture

The adult hippocampal neural stem/progenitors used in this study were originally isolated from adult (8–10 wks old) female Fisher 344 rats and have been characterized previously 26. These progenitor cells were cultured in N2-FGF growth medium [DMEM:F12 with N2 supplement (Invitrogen) and basic fibroblast growth factor (20 ng/ml FGF-2)] and induced to differentiate into oligodendrocytes in the presence of IGF-1 (100 ng/ml).

For mouse oligodendroglial precursor culture, cortical precursors were isolated from embryos at E15.5 and were grown in the N2-bFGF growth medium to enrich Olig2+ OPCs as previously indicated 32, then passaged by trypsinization and cultured in oligodendrocyte growth medium (N2 supplemented with 20 ng/ml FGF2 and 10 ng/ml PDGF-AA)33. An oligodendrocyte differentiation medium [N2 supplemented with 400 ng/ml Triiodothyronine T3 and 20 ng/ml ciliary neurotrophic factor (CNTF)] was used to promote oligodendrocyte differentiation 33, 48. Primary rat OPCs were isolated from P1-2 Sprague Dawley rats as described previously 33.

Transient transfection and immunohistochemistry

Adult rat hippocampus-derived neural progenitor cells (HCN) were seeded and grown in Dulbecco's modified Eagle medium with N2 supplemented with IGF1 (100 ng/ml) before transfection with Amara according to the manufacturer's protocol (*Roche Applied Science, Indianapolis, IN*) and assayed 72-hour post-transfection for immunocytochemistry. Primary rat OPCs were transfected with either *GPR17*-expression or control vector using the NeuroFECT according to the manufacturer's protocol (Genlantis, San Diego, CA). On the next day, OPCs were trypsinized and seeded onto established astrocytes. 3–5 days after seeding, cells were fixed and the progression of transfected OPCs was analyzed by immunocytochemistry. Transfected cells were identified by co-expressed GFP. The immunohistochemical staining procedure was performed as described previously 19. Antibodies used: Olig1, Olig2 (gift of Chuck Stiles), MBP and Neurofilament SMI312 (Covance), Myc (Covance), O4, CNPase, MAG and MOG (Roche), PDGFR α (BD Bioscience), ID2 (BD Bioscience), ID4, GFAP and Myc (Santa Cruz), CC1 (Oncogene research) and Caspase-3 cleaved form (Upstate). Monoclonal antibody to RIP was obtained from the Developmental Studies Hybridoma Bank at the University of Iowa under the auspices of the National Institute of Child Health and Human Development.

Western blotting and nuclear/cytoplasmic fractionation

For protein blotting analysis, whole cell lysates were prepared from HCN cells using RIPA buffer (Tris-HCl, 50 mM, pH 7.4; NP-40, 1%; Na-deoxycholate, 0.25%; NaCl, 150 mM; EDTA, 1 mM; PMSF, 1 mM; aprotinin, leupeptin, pepstatin, 1 mg/ml; Na₃VO₄, 1 mM; NaF, 1 mM). For nuclear and cytoplasmic extracts, HCNs were lysed in hypotonic buffer (Hepes, 10 mM, pH8; MgCl₂, 1.5 mM; KCl, 10 mM; DTT, 1mM). Nuclei was then isolated and resuspended in the same buffer with NaCl, 420 mM; EDTA, 0.2 mM; glycerol, 25%; NP-40, 1%; PMSF, 1 mM; aprotinin, leupeptin, pepstatin, 1 mg/ml. Protein concentration in centrifugation-clarified cell lysates were measured by the BCA Protein Assay Kit (Pierce) and equal amounts of protein were separated on a 4–12% SDS-PAGE and transferred to Hybond PVDF (Amersham Biosciences). Protein blots were done using the NuPage gel transfer system with 4–20% Tris-Bis gels (Invitrogen). Primary Abs for protein blotting included: mouse anti-GAPDH (1:5000; Chemicon), rabbit anti-ID2 (1:500; Santa Cruz); rabbit anti-CREB (1:100; Cell Signaling). Immunoreactive bands were visualized using HRP-conjugated secondary antibodies, followed by ECL (Amersham Biosciences).

Chromatin immunoprecipitation (ChIP)

Chromatin was isolated from 1×10^7 rat hippocampus neural progenitor cells that were transfected either with empty vector containing Myc-nls-Tag or vector expressing Myc-nls-tag fused Olig1. After immunoprecipitation with $5 \mu\text{g}$ anti-Myc antibody (mouse monoclonal sc-40X, Santa Cruz), chromatin was reverse cross-linked using EZ ChIP kit (Upstate Biotechnology). Proteins were digested with proteinase K and the recovered DNA was purified using QIAGEN QIAquick PCR purification kit and subjected to PCR amplification. PCR primers for ChIP assays were designed to amplify around 200 bp fragments from the upstream of start site of *GPR17* containing with or without E-box (CANNTG) consensus sequences for bHLH protein binding. Real-time PCR was carried out using quantitative SYBR green PCR mix (Applied Biosystems, Inc.). The fold-enrichments were determined by the 2^{-CT} methods as previously described 49. Primer sequences are for region I: forward 5'-ccaacgtaaagtagccagtctctgg-3', reverse 5'-gctggtaactctattgtgaccagc-3'; Region II: forward 5'-aggtagctttccaggctctgagtt-3', reverse 5'-aactcgggagaaacatggctgttc-3'.

Induction of EAE

EAE was induced in 6–8 week old C57/BL6 mice (Taconic, NY) by s.c. injection over 2 sites in the flanks with $200 \mu\text{g}$ MOG35–55 (MEVGWYRSPFSRVVHLYRNGK) emulsified in CFA, supplemented with *M. tuberculosis* (4mg/ml) (Difco, Detroit, MI). Pertussis toxin ($200 \text{ ng}/\text{mouse}$) in PBS was injected i.p. at the time of immunization and 48 h later. Mice were scored on scale of 0 to 6 as previously described 50: 0, no clinical disease; 1, limp/flaccid tail; 2, moderate hind limb weakness; 3, severe hind limb weakness; 4, complete hind limb paralysis; 5 quadriplegia or premoribund state; 6, death. Animal use and studies were approved by the Institutional Animal Care and Use Committee of the University of Texas Southwestern Medical Center at Dallas.

Analysis of human MS samples

Tissue specimens from MS patients were obtained from the Human Brain and Spinal Fluid Resource Center, VA West Los Angeles Healthcare Center, Los Angeles, CA 90073 which is sponsored by NINDS/NIMH, National Multiple Sclerosis Society, and Department of Veterans Affairs. Frozen autopsy samples from 10 MS and 10 normal control cases were processed for total RNA using Qiagen RNeasy, with adjacent sections being processed for histology (H&E). For each MS donor, samples included plaques, adjacent white matter, and nearest grey matter; all samples were from frontal lobe.

Total RNA was assessed for quality by Agilent Bioanalyzer and expression of huGPR17 was measured by quantitative real-time RT-PCR using the ABI PRISM 7900HT sequence detection system (Applied Biosystems, Inc.) and normalized to the expression of a housekeeping gene (HPRT). Two unique qPCR primer/probe sets (5'-3') were used to determine relative expression of *Gpr17* cDNA and confirm expression patterns. All RNA was DNase-treated (DNA-free, Ambion) prior to generation of cDNA using a Taqman reverse transcription kit (Applied Biosystems Inc). Using 20 ng of total RNA equivalent cDNA, samples were subject to qPCR using 2x Taqman Universal Buffer (Applied Biosystems Inc.) with $200 \mu\text{M}$ forward and reverse primers and $900 \mu\text{M}$ probe with the following PCR conditions 50°C for 2 min; 95°C for 10 min; 95°C for 15 s; 60°C for 1 min

(40x). Each PCR reaction was run in triplicate for each biological sample included in the study.

Statistical analysis

Results were analyzed for statistical significance using two-tailed Student's *t* test and all error bars were expressed as standard deviations (SD). Values of $p < 0.05$ were considered significant. For multiple comparisons, which were done using one-way analysis of variance analysis (ANOVA) with posttest: Newman-Keuls Multiple comparison test.

Supplementary Material

Refer to Web version on PubMed Central for supplementary material.

Acknowledgements

Authors thank C. Stiles, J. Chan, J. Johnson, R. Bassel-Duby, E. Hurlock and T. Hu for critical comments, M. Gravel for CNP1 promoter, M. Yanagisawa for ligand analysis, J. Koch for preliminary injury study, J. Cai, T. Hu, X. Xu and T. Yue for technical assistance, L. Cai for microarray analysis, T. Januszewski and L. Mueller for electron microscopy. This study was funded by grants from the National Institutes of Health (NS050389 to QRL) and the National Multiple Sclerosis Society (RG3978 to QRL and RG2891 to AG). QRL is a Harry Weaver Neuroscience Scholar.

References

1. Trapp BD, et al. Axonal transection in the lesions of multiple sclerosis. *N Engl J Med.* 1998; 338:278–285. [PubMed: 9445407]
2. Berger J, Moser HW, Forss-Petter S. Leukodystrophies: recent developments in genetics, molecular biology, pathogenesis and treatment. *Curr Opin Neurol.* 2001; 14:305–312. [PubMed: 11371752]
3. Pfeiffer SE, Warrington AE, Bansal R. The oligodendrocyte and its many cellular processes. *Trends in Cell Biology.* 1993; 3:191–197. [PubMed: 14731493]
4. Wang S, Sdrulla A, Johnson JE, Yokota Y, Barres BA. A role for the helix-loop-helix protein Id2 in the control of oligodendrocyte development. *Neuron.* 2001; 29:603–614. [PubMed: 11301021]
5. Kondo T, Raff M. The Id4 HLH protein and the timing of oligodendrocyte differentiation. *Embo J.* 2000; 19:1998–2007. [PubMed: 10790366]
6. Durand B, Raff M. A cell-intrinsic timer that operates during oligodendrocyte development. *Bioessays.* 2000; 22:64–71. [PubMed: 10649292]
7. Dugas JC, Ibrahim A, Barres BA. A crucial role for p57(Kip2) in the intracellular timer that controls oligodendrocyte differentiation. *J Neurosci.* 2007; 27:6185–6196. [PubMed: 17553990]
8. Casaccia-Bonnel P, et al. Loss of p27Kip1 function results in increased proliferative capacity of oligodendrocyte progenitors but unaltered timing of differentiation. *Development.* 1999; 126:4027–4037. [PubMed: 10457012]
9. Nave KA, Salzer JL. Axonal regulation of myelination by neuregulin 1. *Curr Opin Neurobiol.* 2006; 16:492–500. [PubMed: 16962312]
10. Vartanian T, Goodearl A, Viehover A, Fischbach G. Axonal neuregulin signals cells of the oligodendrocyte lineage through activation of HER4 and Schwann cells through HER2 and HER3. *J Cell Biol.* 1997; 137:211–220. [PubMed: 9105049]
11. Wang S, et al. Notch receptor activation inhibits oligodendrocyte differentiation. *Neuron.* 1998; 21:63–75. [PubMed: 9697852]
12. Hu QD, et al. F3/contactin acts as a functional ligand for Notch during oligodendrocyte maturation. *Cell.* 2003; 115:163–175. [PubMed: 14567914]
13. Mi S, et al. LINGO-1 negatively regulates myelination by oligodendrocytes. *Nat Neurosci.* 2005; 8:745–751. [PubMed: 15895088]

14. Samanta J, Kessler JA. Interactions between ID and OLIG proteins mediate the inhibitory effects of BMP4 on oligodendroglial differentiation. *Development*. 2004; 131:4131–4142. [PubMed: 15280210]
15. Levine JM, Reynolds R. Activation and proliferation of endogenous oligodendrocyte precursor cells during ethidium bromide-induced demyelination. *Exp Neurol*. 1999; 160:333–347. [PubMed: 10619551]
16. Chang A, Nishiyama A, Peterson J, Prineas J, Trapp BD. NG2-positive oligodendrocyte progenitor cells in adult human brain and multiple sclerosis lesions. *J Neurosci*. 2000; 20:6404–6412. [PubMed: 10964946]
17. Yue T, et al. A critical role for dorsal progenitors in cortical myelination. *J Neurosci*. 2006; 26:1275–1280. [PubMed: 16436615]
18. Arnett HA, et al. bHLH transcription factor Olig1 is required to repair demyelinated lesions in the CNS. *Science*. 2004; 306:2111–2115. [PubMed: 15604411]
19. Xin M, et al. Myelination and axonal recognition by oligodendrocytes in brain are uncoupled in Olig1-null mice. *J Neurosci*. 2005; 25:1354–1365. [PubMed: 15703389]
20. Zhou Q, Anderson DJ. The bHLH transcription factors OLIG2 and OLIG1 couple neuronal and glial subtype specification. *Cell*. 2002; 109:61–73. [PubMed: 11955447]
21. Lu QR, et al. Common developmental requirement for Olig function indicates a motor neuron/oligodendrocyte connection. *Cell*. 2002; 109:75–86. [PubMed: 11955448]
22. Li H, Lu Y, Smith HK, Richardson WD. Olig1 and Sox10 interact synergistically to drive myelin basic protein transcription in oligodendrocytes. *J Neurosci*. 2007; 27:14375–14382. [PubMed: 18160645]
23. Wang SZ, et al. An oligodendrocyte-specific zinc-finger transcription regulator cooperates with Olig2 to promote oligodendrocyte differentiation. *Development*. 2006; 133:3389–3398. [PubMed: 16908628]
24. Parravicini C, Ranghino G, Abbracchio MP, Fantucci P. GPR17: Molecular modeling and dynamics studies of the 3-D structure and purinergic ligand binding features in comparison with P2Y receptors. *BMC Bioinformatics*. 2008; 9:263. [PubMed: 18533035]
25. Campagnoni, AT. Molecular biology of myelination. In: Kettenmann, H.; Ransom, BR., editors. *Neuroglia*. New York: Oxford University Press; 2005. p. 253-267.
26. Hsieh J, et al. IGF-I instructs multipotent adult neural progenitor cells to become oligodendrocytes. *J Cell Biol*. 2004; 164:111–122. [PubMed: 14709544]
27. Nave KA. Neurological mouse mutants and the genes of myelin. *J Neurosci Res*. 1994; 38:607–612. [PubMed: 7807578]
28. Cai J, et al. A crucial role for Olig2 in white matter astrocyte development. *Development*. 2007; 134:1887–1899. [PubMed: 17428828]
29. Ito D, et al. Microglia-specific localisation of a novel calcium binding protein, Iba1. *Brain Res Mol Brain Res*. 1998; 57:1–9. [PubMed: 9630473]
30. Megason SG, McMahon AP. A mitogen gradient of dorsal midline Wnts organizes growth in the CNS. *Development*. 2002; 129:2087–2098. [PubMed: 11959819]
31. Marin-Husstege M, et al. Multiple roles of Id4 in developmental myelination: predicted outcomes and unexpected findings. *Glia*. 2006; 54:285–296. [PubMed: 16862533]
32. Gabay L, Lowell S, Rubin LL, Anderson DJ. Deregulation of dorsoventral patterning by FGF confers trilineage differentiation capacity on CNS stem cells in vitro. *Neuron*. 2003; 40:485–499. [PubMed: 14642274]
33. Chen Y, et al. Isolation and culture of rat and mouse oligodendrocyte precursor cells. *Nat Protoc*. 2007; 2:1044–1051. [PubMed: 17546009]
34. Ross SE, Greenberg ME, Stiles CD. Basic helix-loop-helix factors in cortical development. *Neuron*. 2003; 39:13–25. [PubMed: 12848929]
35. Gokhan S, et al. Combinatorial profiles of oligodendrocyte-selective classes of transcriptional regulators differentially modulate myelin basic protein gene expression. *J Neurosci*. 2005; 25:8311–8321. [PubMed: 16148239]

36. Chang A, Tourtellotte WW, Rudick R, Trapp BD. Premyelinating oligodendrocytes in chronic lesions of multiple sclerosis. *N Engl J Med*. 2002; 346:165–173. [PubMed: 11796850]
37. Franklin RJ. Why does remyelination fail in multiple sclerosis? *Nat Rev Neurosci*. 2002; 3:705–714. [PubMed: 12209119]
38. John GR, et al. Multiple sclerosis: Re-expression of a developmental pathway that restricts oligodendrocyte maturation. *Nat Med*. 2002; 8:1115–1121. [PubMed: 12357247]
39. Cahoy JD, et al. A transcriptome database for astrocytes, neurons, and oligodendrocytes: a new resource for understanding brain development and function. *J Neurosci*. 2008; 28:264–278. [PubMed: 18171944]
40. Lecca D, et al. The recently identified P2Y-like receptor GPR17 is a sensor of brain damage and a new target for brain repair. *PLoS ONE*. 2008; 3:e3579. [PubMed: 18974869]
41. Ciana P, et al. The orphan receptor GPR17 identified as a new dual uracil nucleotides/cysteinyl-leukotrienes receptor. *Embo J*. 2006; 25:4615–4627. [PubMed: 16990797]
42. Durand B, Gao FB, Raff M. Accumulation of the cyclin-dependent kinase inhibitor p27/Kip1 and the timing of oligodendrocyte differentiation. *Embo J*. 1997; 16:306–317. [PubMed: 9029151]
43. Tokumoto YM, Apperly JA, Gao FB, Raff MC. Posttranscriptional regulation of p18 and p27 Cdk inhibitor proteins and the timing of oligodendrocyte differentiation. *Dev Biol*. 2002; 245:224–234. [PubMed: 11969268]
44. Casaccia-Bonnel P, et al. Oligodendrocyte precursor differentiation is perturbed in the absence of the cyclin-dependent kinase inhibitor p27Kip1. *Genes Dev*. 1997; 11:2335–2346. [PubMed: 9308962]
45. Lu QR, et al. Sonic hedgehog--regulated oligodendrocyte lineage genes encoding bHLH proteins in the mammalian central nervous system. *Neuron*. 2000; 25:317–329. [PubMed: 10719888]
46. Gow A, Friedrich VL, Lazzarini RA. Myelin basic protein gene contains separate enhancers for oligodendrocyte and Schwann cell expression. *J Cell Biol*. 1992; 119:605–616. [PubMed: 1383235]
47. Gravel M, Di Polo A, Valera PB, Braun PE. Four-kilobase sequence of the mouse CNP gene directs spatial and temporal expression of lacZ in transgenic mice. *J Neurosci Res*. 1998; 53:393–404. [PubMed: 9710259]
48. Barres BA, Lazar MA, Raff MC. A novel role for thyroid hormone, glucocorticoids and retinoic acid in timing oligodendrocyte development. *Development*. 1994; 120:1097–1108. [PubMed: 8026323]
49. Bernstein BE, et al. A bivalent chromatin structure marks key developmental genes in embryonic stem cells. *Cell*. 2006; 125:315–326. [PubMed: 16630819]
50. Karandikar NJ, et al. Tissue-specific up-regulation of B7-1 expression and function during the course of murine relapsing experimental autoimmune encephalomyelitis. *J Immunol*. 1998; 161:192–199. [PubMed: 9647224]

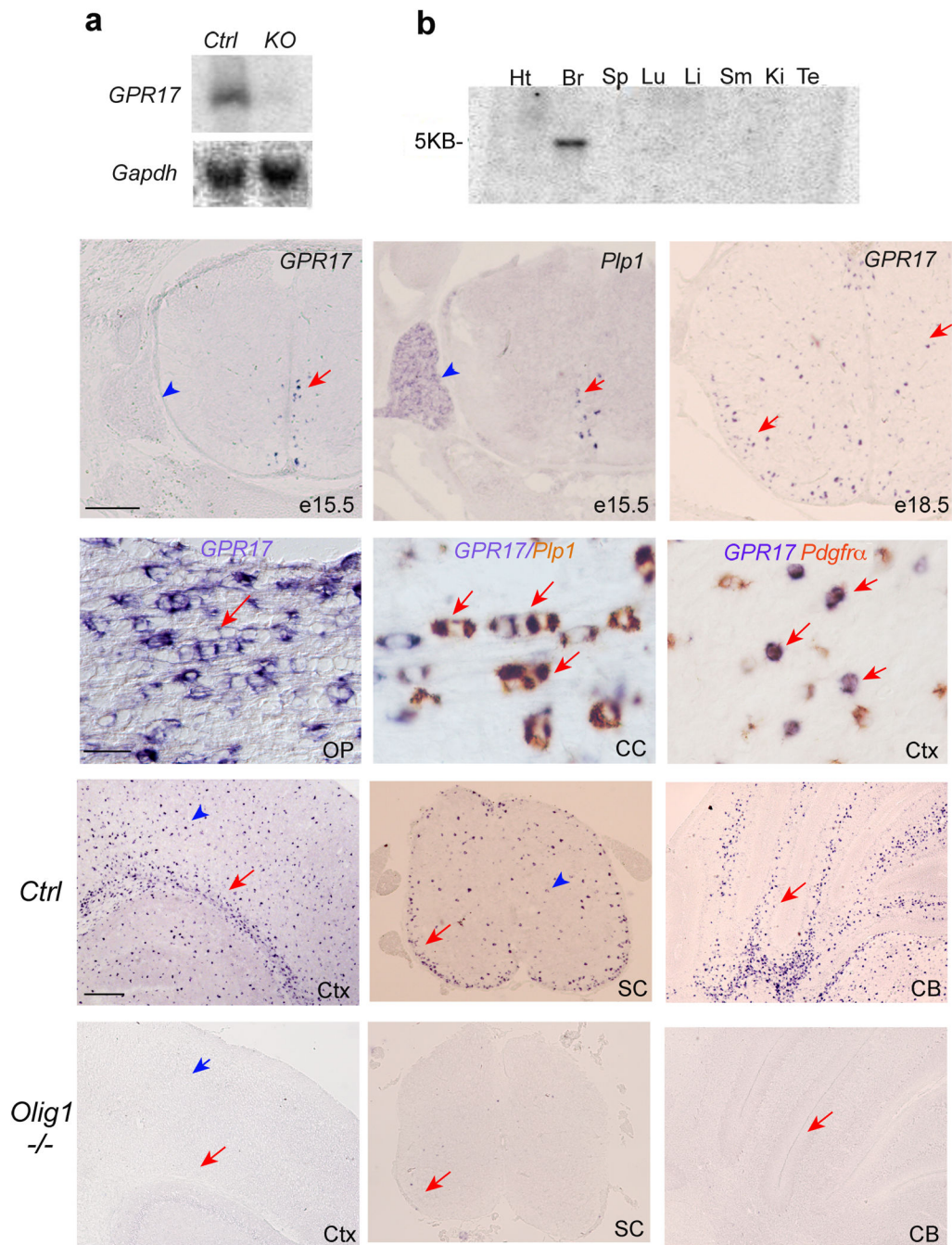


Figure 1. Identification and expression of *GPR17* in the murine CNS

a) Upper panel, a Northern blot of RNA extracted from brain tissues of WT and *Olig1* mutant mice at P14 was probed with ^{32}P -labeled *GPR17*. Lower panel, expression of a housekeeping gene *Gapdh* from the same samples above was used as loading controls. **b)** A commercial Northern blot (Clontech) of mRNA extracted from various rat tissues was probed with ^{32}P -labeled *GPR17*, revealing 5kb mRNA transcript in the brain. **c-f)** *In situ* hybridization was performed with probes specific for *GPR17* and *Plp1/DM20* in e15.5 (**c-d**) and e18.5 (**e**) spinal cords and P14 (**f**) optic nerve in mice. Arrows indicate labeled cells.

Arrowheads indicate dorsal root ganglia. **g–h**) Double *in situ* hybridization labeling for *GPR17* (blue color) and *Plp1* (brown color) or *Pdgfra* (brown color) at P14. Arrows indicate a linear array of interfascicular oligodendrocytes expressing both *GPR17* and *Plp1* in the corpus callosum (**g**). Arrows in **h** indicate *GPR17* expression in a subset of PDGFR α + OPCs in the cerebral cortex. **i–n**) Expression of *GPR17* mRNA in various CNS regions of WT (**i–k**) and *Olig1KO* (**l–n**) mice at P14. Arrows and arrowheads indicate labeling cells in white matter tracts and grey matter regions, respectively. SC, spinal cord; CB, cerebellum; OP, optic nerve; CC, corpus callosum; Ctx, cortex. Scale bars in **c–e**: 200 μ m; **f–h**, 100 μ m; **i–n**: 200 μ m.

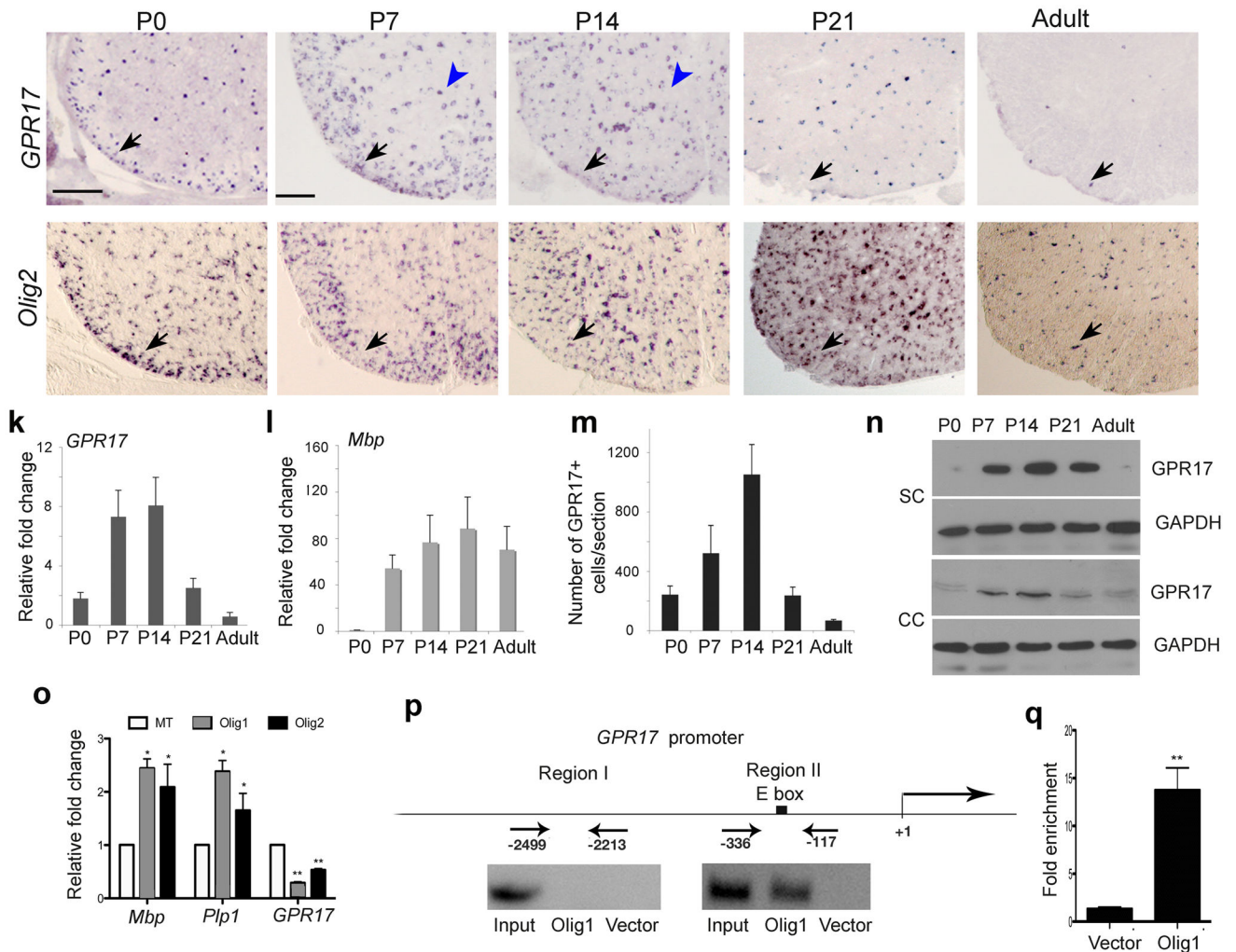


Figure 2. Transient expression of *GPR17* in oligodendrocytes during development
a–j) *In situ* hybridization on transverse spinal cord sections from P0, P7, P14, P21 and adulthood with probes to murine *GPR17* and *Olig2* as indicated. Arrows and arrowheads indicate *GPR17* or *Olig2* positive cells in the spinal white or gray matter, respectively. **k–l)** Transcripts of *GPR17* (**k**) and *Mbp* (**l**) were determined in total RNA prepared from spinal cords at different stages by qRT-PCR (n=3). **m)** Average number of *GPR17*⁺ cells per spinal section at the indicated age. *GPR17*⁺ cell number was counted from at least 5 sections at the thoracic level of each animal (n=3). **n)** Western blot analysis of *GPR17* protein from the spinal cord and corpus callosum at indicated stages. GAPDH was used as a loading control for protein extracts. **o)** qRT-PCR analysis of *GPR17*, *Mbp* and *Plp1* transcript in adult hippocampus-derived neural stem/progenitor cells (HCN) transfected with pCS2MT-nls-*Olig1*, *Olig2* or control expression vector. The fold change of gene expression was present from cells transfected with *Olig1* or *Olig2* versus control (*P<0.01, **P<0.001, Student t-test). **p)** Recruitment of *Olig1* to the *GPR17* 5' upstream regulatory sequence. Regions upstream the start site of *GPR17* with E-box (Region II) or without E-Box (Region I) consensus sequences were amplified with specific PCR primers for ChIP assay. Input

DNA was used as positive control. **q)** Quantification of ChIP enrichment of Olig1 binding to E-box containing region II in the *GPR17* promoter by qRT-PCR in *Olig1*-transfected cells compared to vector-transfected cells (**P<0.001, Student t-test). Scale bars in **a–j**: 200 μ m.

Author Manuscript

Author Manuscript

Author Manuscript

Author Manuscript

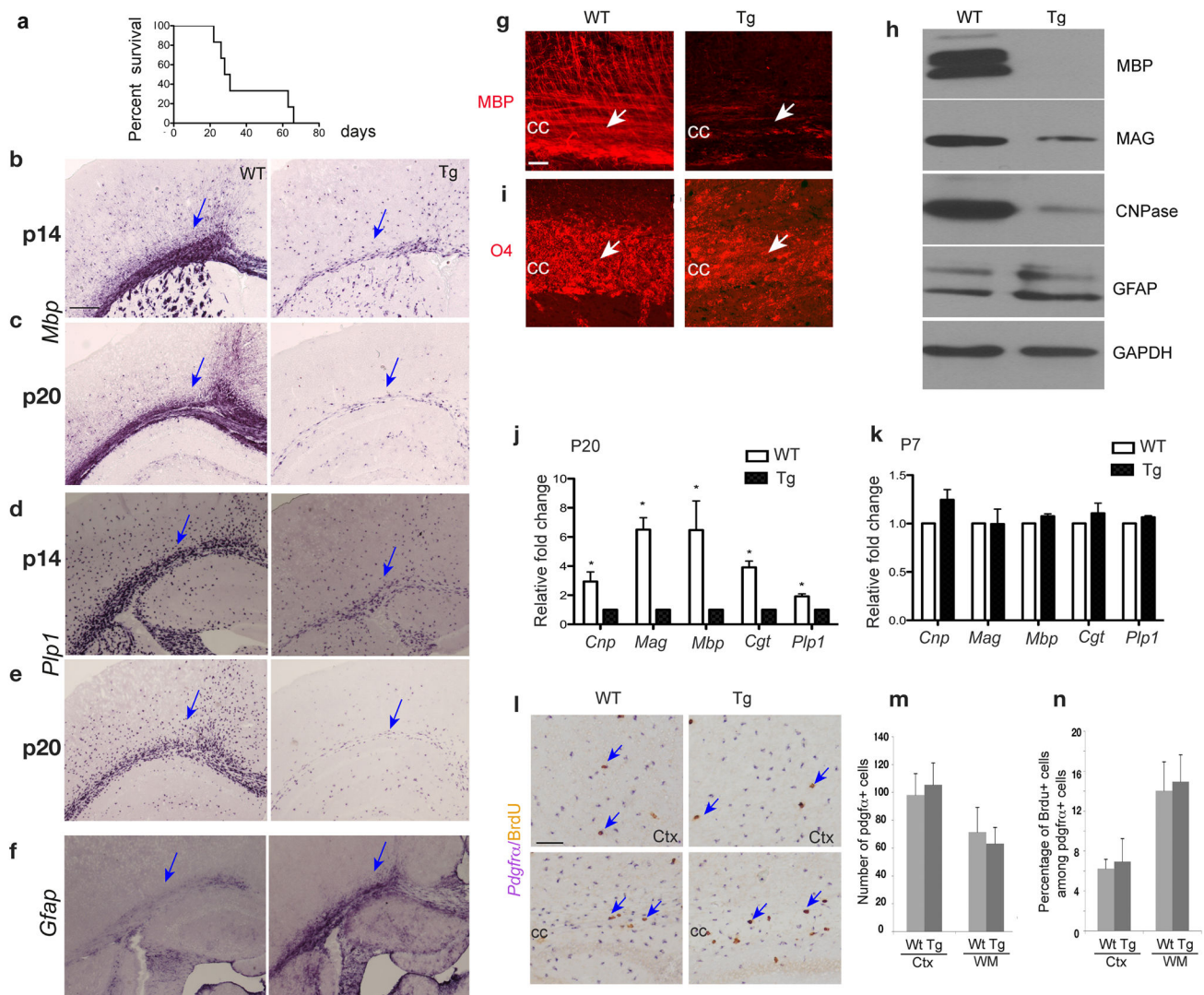


Figure 3. Deficiency of myelin gene expression in the brain of *GPR17* transgenic animals
a) Life span assessment shows the majority of *CNPI-GPR17* transgenic mice die around postnatal 3–4 weeks (17/23 examined). A few (6/23) transgenic mice can barely survive to the adulthood. **b–f)** In situ hybridization was performed with antisense riboprobes against *Mbp*, *Plp1* and *Gfap* on the forebrain of WT and *GPR17* transgenic (Tg) littermates at P14 and P20. Arrows indicate the white matter. **g, i)** Immunohistochemistry was performed with antibodies against MBP and O4 on the corpus callosum (CC, arrows) sections from WT and Tg littermates at P20. **h)** Western blot analysis of MBP, MAG, CNPase and GFAP on the tissues from the forebrain of WT and Tg littermates at P19. **j–k)** Expression of *Cnp*, *Mag*, *Mbp*, *Cgt* and *Plp1* was determined using total RNAs prepared from the forebrain of WT and Tg littermates at P7 and P20 by qRT-PCR from three independent experiments. Values were normalized to GAPDH for each sample. * $P < 0.01$ (Student *t*-test). **l)** Cycling OPCs in the brain were determined by double in situ hybridization and immunohistochemistry 4 h after BrdU administration to animals at P14. BrdU⁺ (brown)/*Pdgfra*⁺ (purple) OPCs are indicated by arrows. **m, n)** The number of *Pdgfra*⁺ OPCs per field (0.08 mm²) (**m**) and the

proportion of BrdU+/*Pdgfra*+ OPCs in the cell cycle (**n**) were quantified from three WT and Tg littermates. cc, corpus callosum; Ctx, cortex. Scale bars: **b–f**, **g**, **i** and **l**, 100 μ m.

Author Manuscript

Author Manuscript

Author Manuscript

Author Manuscript

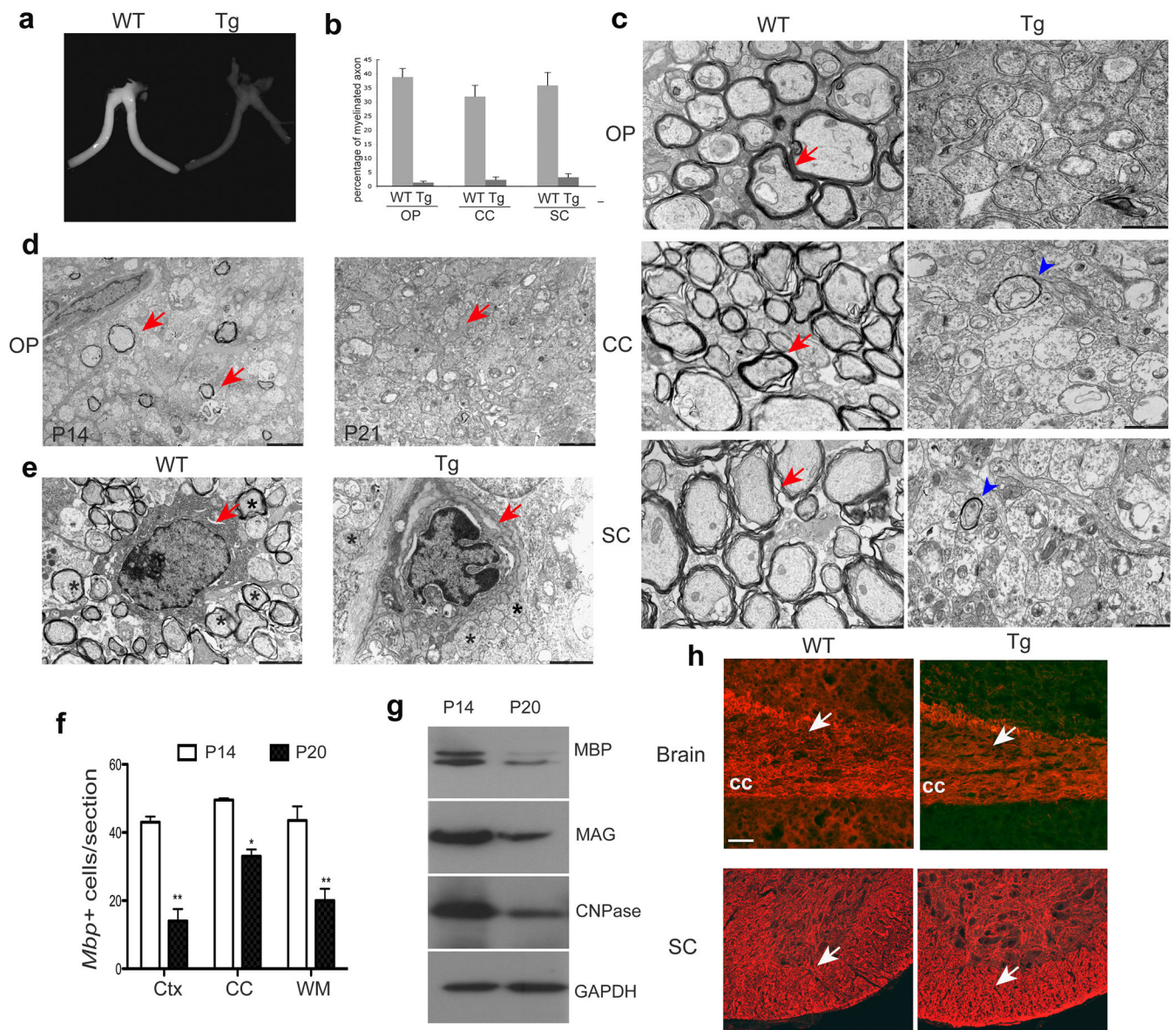


Figure 4. Myelinogenesis defects in the CNS of *CNP-GPR17* transgenic mice

a) Optic nerves isolated from WT mice at P19. **b)** Quantification of the proportion of myelinating axons from the optic nerve, corpus callosum and spinal cord at P19 (>800 axons scored). **c)** Electron micrographs of the optic nerve, corpus callosum and spinal cord in cross-sections from WT and Tg mice at P19. Arrows and arrowheads indicate myelin sheaths. **d)** Electron micrographs of cross-sections of optic nerves from Tg mice at P14 and P21. Arrows indicate myelinated axons, which are absent in the optic nerve of P21 Tg animals. **e)** Ultrastructural analysis showing an apoptotic oligodendrocyte in optic nerves of Tg mice, but a healthy oligodendrocyte in WT mice at P16 (Arrows). Asterisks indicate myelinated axons in WT and unmyelinated axons in Tg mice. **f)** *Mbp* expression on brain sections of Tg mice at P14 and P20 was detected by in situ hybridization. The number of *Mbp*+ oligodendrocytes per field (0.08 mm²) at corresponding regions was quantified in the

corpus callosum (CC), cortex (Ctx), and white matter (WM). * $P < 0.01$, ** $P < 0.001$ (Student *t*-test, $n=3$). **g**) Western blot analysis of MBP, MAG, CNPase from the forebrain of Tg mice at P14 and P20. GAPDH as a control. **h**) The sections from the brain and spinal cord of WT and Tg mice at P20 were immunostained with Neurofilament (red). Arrows indicate the corpus callosum and spinal white matter, respectively. Scale bars in **c–e**, 1 μm ; **h**: 50 μm .

Author Manuscript

Author Manuscript

Author Manuscript

Author Manuscript

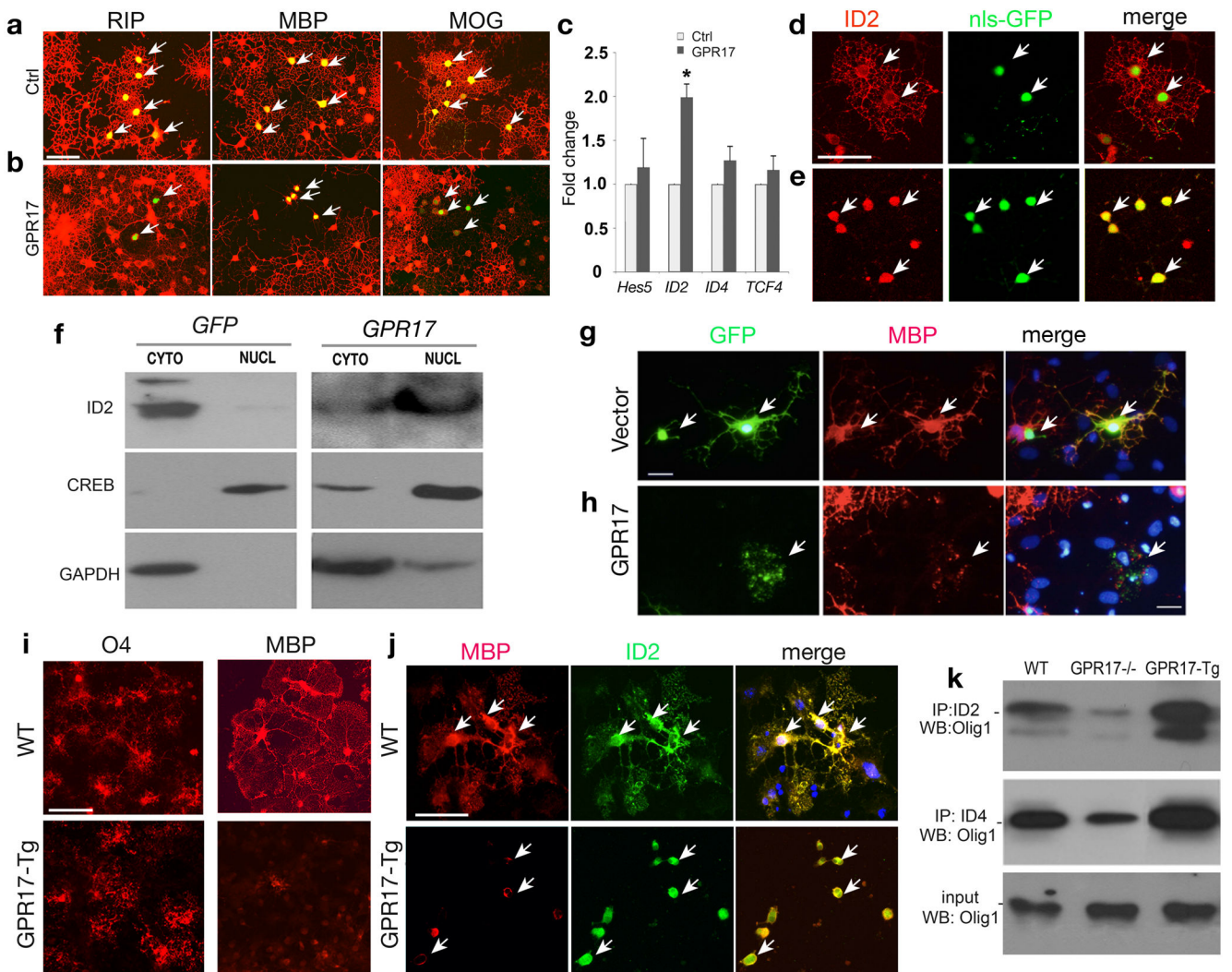


Figure 5. GPR17 overexpression inhibits oligodendrocyte differentiation and induces nuclear translocation of ID2/4

a–b) HCN cells were transfected with *GPR17* and control vector carrying GFP and assayed after 72 hrs and immunostained for RIP, MBP and MOG. Arrows indicate the transfected cells. **c)** Total RNAs extracted from HCN cells transfected with control and *GPR17* were subjected to qRT-PCR analysis for *Hes5*, *ID2*, *ID4* and *TCF4*. * $P < 0.01$ (Student *t*-test). **d–e)** HCN cells transfected with *GPR17* (**e**) or control pCIG (**d**) carrying nuclear-localized GFP (nls-GFP) were immunostained for ID2. Arrows indicate ID2 immunoreactivity in control- or *GPR17*-transfected cells, respectively. **f)** Cytoplasmic (CYTO) and nuclear (NUCL) fractions were prepared 3 days after transfection and subjected to Western blotting analysis for cellular localization of ID2, CREB or GAPDH. **g–h)** Primary rat OPCs transfected with control or *GPR17*-expression vector were co-cultured with astrocytes for 5 days and subjected to immunocytochemistry for MBP and GFP. Arrows in **g, h** indicate MBP⁺ cells in control- or *GPR17*-transfected cells. **i–j)** Cortical progenitors from WT and *GPR17*-Tg embryos at E15.5 were cultured to promote oligodendrocyte formation. Cells were immunostained with antibodies to O4, MBP and ID2 as indicated. Arrows in **j** indicate MBP

or ID2 expression. **k)** Cortical progenitor cells from WT, *GPR17*^{-/-} and *CNP1-GPR17* transgenic embryos at E15.5 were cultured to promote oligodendrocyte formation. The cells were collected and processed for co-immunoprecipitation with an antibody against ID2 or ID4. Immunoprecipitated proteins were subjected to Western blot analysis for Olig1 as indicated. Scale bars in **a–e**, 50 μ m; **g–h**, 25 μ m and **i–j**, 50 μ m.

Author Manuscript

Author Manuscript

Author Manuscript

Author Manuscript

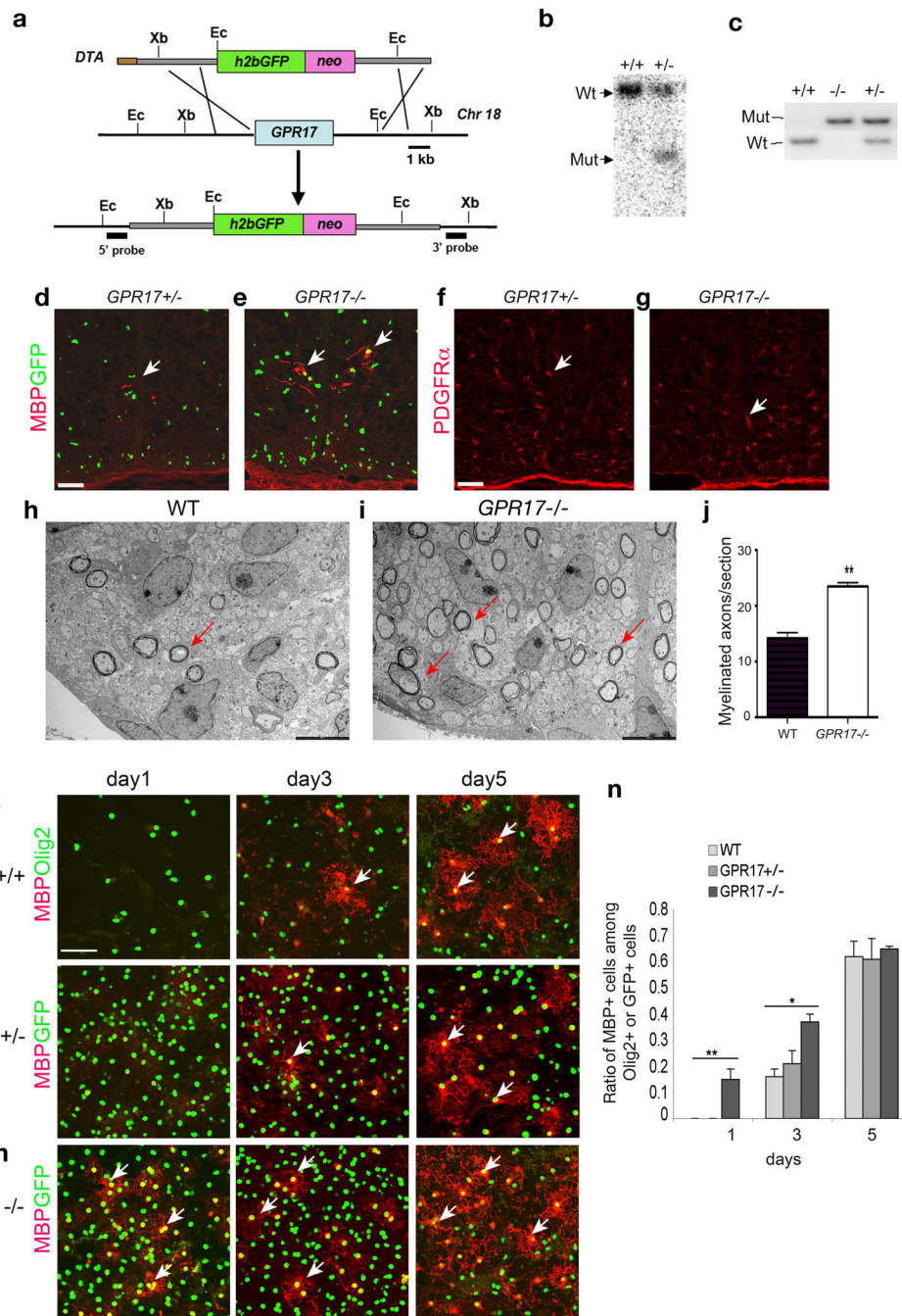


Figure 6. Early onset of oligodendrocyte myelination in *GPR17* null mice

a) Schematic strategy for disruption of *GPR17* on the mouse chromosome 18.

Abbreviations: h2bGFP, histone2b GFP; neo, the neomycin selection marker; and DTA, the diphtheria toxin gene. Ec: EcoRI, Xb: XbaI. **b)** Southern blot validation with a 5' *GPR17* probe identified the targeted locus as a following EcoRI digestion of genomic DNAs. **c)** PCR genotyping analysis of WT and targeted allele from WT, *GPR17*^{+/-} and *-/-* animals. **d–g)** Sections from the spinal cord of *GPR17*^{+/-} and *-/-* embryos at E17.5 were immunostained for MBP (**d, e**) and PDGFR α (**f, g**). Arrows indicate MBP⁺ and PDGFR α ⁺

cells, respectively. **h–i**) Electron micrographs of spinal cross-sections of WT and *GPR17*^{-/-} mice at P3. Arrows indicate multilamellar myelin sheaths around axons in the lateral white matter. **j**) Quantitative analysis of myelinated axon fibers in *GPR17*^{-/-} and WT mice at P3 in the corresponding region of lateral white matter of spinal cord (**P<0.001, Student *t*-test). **k–m**) Cortical progenitor cells from WT, *GPR17*^{+/-} and ^{-/-} embryos at E15.5 were cultured to promote oligodendrocyte differentiation. Cells were then immunostained at defined days as indicated for MBP (arrows) and GFP (**l–m**) or Olig2 (**k**). **n**) Quantification of cells expressing MBP from above cultures. All data shown are derived from three experiments in parallel cultures of at least three age-matching littermates (> 1500 cell counts at each stage). Error bars represent SDs. **p<0.001, One-way ANOVA with Newman-Keuls Multiple comparison test. Scale bars: **d–g**, 100 μm; **h–i**, 1 μm and **k–m**, 50 μm.